The Effects of Dopants on the Cu-ZrO_2 Catalysed Hydrogenation of Levulinic Acid

Jun Hirayama[a,b,c], Igor Orlowski[c], Sarwat Iqbal[c], Mark Douthwaite[c], Satoshi Ishikawa[b,c], Peter J. Miedziak[c], Jonathan K. Bartley[c], Jennifer Edwards[c], Qian He[c], Robert L. Jenkins[c], Toru Murayama[e], Christian Reece[c], Wataru Ueda[b,d], David J. Willock,[c,*] and Graham J. Hutchings[c,*]

[a] Research Fellow of Japan Society for the Promotion of Science (JSPS), 5-3-1 Chiyoda-ku, Tokyo 102-0083, Japan

[b] Faculty of Environmental Earth Science, Hokkaido University, Nishi 5, Kita 10, Kita-ku, Sapporo 060-0810, Japan

[c] Cardiff Catalysis Institute, School of Chemistry, Cardiff University, Main Building, Park Place, Cardiff CF10 3AT, U.K.

[d] Department of Material and Life Chemistry, Faculty of Engineering, Kanagawa University, 3-27, Rokkakubashi, Kanagawa-ku, Yokohama, 221-8686, Japan

[e] Research Center for Gold Chemistry, Tokyo Metropolitan University, 1-1-203, Minami-Osawa, Hachioji, 192-0397, Japan

*E-mail: willockdj@cardiff .ac.uk, hutch@cardiff .ac.uk

Abstract

Catalytic hydrogenation of levulinic acid to form γ-valerolactone was studied over Cu-ZrO_2 catalysts doped with metal oxides from the first row transition metals. The Cu-ZrO_2 material was prepared by oxalate gel co-precipitation and dopants were added by an incipient wetness approach. The addition of 1% Mn into Cu-ZrO_2 significantly increases the yield of γ-valerolactone and the catalytic activity of Mn/Cu-ZrO_2 was found to be 1.6 times higher than that of the undoped Cu-ZrO_2 catalyst. Catalyst characterization suggests that the Mn dopant improves the dispersion of Cu on the surface of ZrO_2. Kinetic studies show that the reaction order with respect to the substrate concentration is approximately zero. However, the order of reaction with respect to the partial pressure of H_2 is different for the Mn/Cu-ZrO_2 and Cu-ZrO_2 catalysts. Comparison of reaction products from reactions carried out in H_2O and D_2O solvents using ^{1}H NMR and ^{13}C NMR show that there is a pre-equilibrium keto-enol isomerisation step under our reaction conditions. DFT calculations show that the enol isomers have a higher affinity for the Cu surface which may improve the availability of the substrate in the hydrogenation step of the reaction.

1. Introduction

Levulinic acid (LA) is an important intermediate for the conversion of non-food biomass into fine chemicals and fuels.[1-3] LA can be transformed into a variety of valuable chemicals such as polymer resins, components of flavoring and fragrance compounds, extenders for fuels, antimicrobial agents, herbicides and more.[4] One of the most important compounds derived from LA is γ-valerolactone (GVL), which has been identified as a suitable target for next-generation biorefineries. GVL has several desirable properties that make it an excellent sustainable feedstock for the production of both energy and carbon-based consumer products.[5-7] Several homogeneous catalyst systems have been reported which give high yields of GVL[8-13], but heterogeneous catalysts are preferred due to the ease of separation of catalyst from the reaction mixture. Typical heterogeneous catalyst systems employed for GVL synthesis from LA consist of noble metal catalysts *e.g.* Ru[14-21], Au[18, 22, 23], Pt[18, 23], and Pd.[18, 23, 24] Amongst these catalysts, supported Ru is the most widely studied because of the ability of Ru to catalyze the hydrogenation of LA under mild reaction conditions (≤ 10 bar H_2, 100°C).[16, 17, 19] As illustrated in Scheme 1, mechanistic studies with Ru/C catalysts show that the conversion of LA, **1**, into GVL, **3**, involves a hydrogenation step to 4-hydroxypentanoic acid (HPA, **2**) and an intramolecular esterification to close the ring in the GVL product.[14] However, the high cost and low abundance of Ru metal has limited its use at a commercial scale. Recently, focus has shifted toward the use of cheaper and more abundant metal catalysts, for example Ni[25-29] and Cu[30-34] catalysts.

We have previously reported that the efficient conversion of LA to GVL can be achieved using a copper–zirconia (Cu-ZrO_2) catalyst prepared either by a co-precipitation from the aqueous nitrate salts[34] or by an oxalate gel co-precipitation method.[31] We found

that the catalytically active components of these Cu–ZrO_2 catalysts for the hydrogenation of LA are reduced Cu nanoparticles dispersed on the surface with a strong interaction with the Cu incorporated into the zirconia support. Even so the conditions required for these Cu based catalysts (200°C, 35 bar)[35] are considerably more exacting than quoted above for a typical Ru catalyst. Hence, there is a need to further improve the activity of Cu-ZrO_2 catalysts so that the experimental temperature and pressure may be lowered.

Herein, we explore the use of first row transition metals as dopants in an attempt to improve the catalytic activity of Cu-ZrO_2 for hydrogenation of LA to GVL. We have characterized the doped catalysts using Scanning electron microscopy (SEM), Transmission electron microscopy (TEM) , X-ray diffraction (XRD), Temperature programmed reduction (TPR), Brauner, Emmette and Teller (BET) surface area measurement, and N_2O titration (metal surface area measurements) in order to relate their catalytic activity with their morphology and physical properties. Mn is identified as the

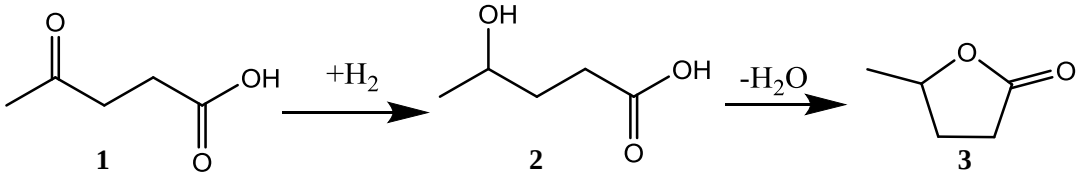

Scheme 1 Hydrogenation of LA to GVL

most promising dopant and we discuss the role of Mn in the resulting Mn/Cu-ZrO_2 catalyst based on material characterization measurements and reaction kinetic studies.

2. Experimental Methods

2.1 Preparation of catalysts

Cu-ZrO_2 catalysts were prepared by the oxalate gel precipitation method.[31] In a typical synthesis 0.01 mol of $Cu(NO_3)_2{\cdot}3H_2O$ (Acros Organics, 99%) and 0.01 mol of $ZrO(NO_3)_2{\cdot}6H_2O$ (Acros Organics, 99.5%) were dissolved in 200 ml of ethanol at room

temperature. Then, 0.024 mol of oxalic acid dihydrate (BDH Chemicals, 99.5%) was added into the mixed metal solution and stirred for 2 h at room temperature. The resultant gel was filtered out and dried at 110 °C overnight. The dried material was calcined at 550 °C for 2 h with a 10 °C min^{-1} ramp under static air. The addition of a secondary metal from the first-row transition metals, M (=Sc to Zn) to give (M/Cu-ZrO_2) was conducted using a wet impregnation method. For wet impregnation, the calcined Cu-ZrO_2 (0.5 g) was dispersed in a metal salt solution of the dopant metal precursor in ethanol (3 ml), and then the resulting slurry was dried under vigorous stirring. The solid was then re-calcined at 550 °C for 2 h with a 10 °C min^{-1} ramp under static air, and then reduced at 300 °C for 2 h with a 10 °C min^{-1} ramp under 5% H_2/Ar mixture gas. The metal precursors used for wet impregnation were $Sc(NO_3)_3 \cdot xH_2O$ (Sigma Aldrich, 99.9%), $TiCl_4$ (Sigma Aldrich, ≥99.0%), VCl_3 (Sigma Aldrich, 97%), $Cr(NO_3)_3 \cdot 9H_2O$ (Sigma Aldrich, 99.99%), $Mn(NO_3)_2 \cdot 4H_2O$ (Sigma Aldrich, 97%), $Fe(NO_3)_3 \cdot 9H_2O$ (Sigma Aldrich, 98%), $Co(NO_3)_2 \cdot 6H_2O$ (Sigma Aldrich, 99.999%), $Ni(NO_3)_2 \cdot 6H_2O$ (Sigma Aldrich, 98.5%), $Cu(NO_3)_2 \cdot 3H_2O$ (Acros Organics, 99%), and $Zn(NO_3)_2 \cdot 6H_2O$ (Sigma Aldrich, 98%).

2.2 Characterization

Powder X-ray diffraction (PXRD) was performed on an X'Pert Pro diffractometer with a monochromatic Cu-Kα source (λ = 0.154 nm) operated at 40 kV and 40 mA. The scans were recorded in the 2θ range between 10° and 80°. Raman spectroscopy was performed on an inVia Raman Microscope (Renishaw) using both 514 nm and 785 nm lasers for powder samples. Total surface areas were determined by multi-point N_2 adsorption at 77 K on a Micromeretics Gemini 2360 according to the Brauner Emmet and Teller (BET) method. Prior to the analyses, samples were degassed at 120 °C for 1 h under N_2 flow.

Temperature programmed reduction (TPR) was carried out on a Thermo 1100 series TPDRO (Quantachrome) equipped with a cold trap with 75 ml min^{-1} of 10%H_2/Ar using a 10 °C min^{-1} ramp rate. Samples (10 mg) were pre-treated at 110 °C under a flow of argon (20 ml min^{-1}) for 20 min prior to reduction in order to clean the surface. Analysis was performed under 10%H_2/Ar (20 ml min^{-1}) flow with 5 °C min^{-1} ramp.

N_2O titration, to determine the Cu surface area, was performed on a ChemBet (Quantachrome) for catalysts after reduction. Prior to the analysis, the catalysts were treated *in situ* under 30 ml min^{-1} of 10%H_2/Ar flow at 180 °C. Then the temperature was reduced to 65 °C with He purging. N_2O was pulsed and detected using a thermal conductivity detector (TCD). After titration, a known amount of N_2 was fed for calibration. A total of 1.46×10^{19} Cu atom m^{-2} and a stoichiometry of $2Cu/N_2$ were used to calculate Cu surface area.[36, 37]

Electron microscopy was performed using a MAIA3 scanning electron microscope (SEM). The powdered samples were dry dispersed onto holey carbon film on copper grids. Energy dispersive X-ray (EDX) analysis was performed using Oxford Instruments X-Max 80 mm^2 SDD. The primary beam energy is set to be 10 keV and the beam current is about 200 pA for both imaging and analysis.

2.3 Hydrogenation of LA to GVL

All experiments were carried out using a 50 ml capacity stainless steel autoclave (Model 5500HP, Parr Instruments) equipped with a Teflon liner and a mechanical stirrer. The reactor was equipped with a gas inlet valve for charging gas into the reactor and a gas release valve for releasing pressure and gas sampling. Unless otherwise stated reactions were carried out under a set of standard conditions; reaction temperature 200 °C, reaction time 0.5 h, and 10 g of 5% LA (Sigma Aldrich, 98%) diluted with distilled water

was used as a substrate, the reaction mixture was stirred at a rate of 2000 rpm. Before the reaction, the reactor was purged three times with 5 bar of nitrogen gas, in order to remove residual air, followed by purging three times with 35 bar of hydrogen. The reactor was then heated to the reaction temperature and the autogeneous pressure this generated noted. The reactor was then pressurized to a total pressure of 35 bar using H_2 at which point the reference zero time for the reaction was set. This procedure resulted in a partial pressure of H_2 of 26.4 bar under the standard reaction conditions. Blank runs, without the catalyst present, showed no LA conversion. Acetonitrile (Acros Organics, 99.9%) was used an internal standard for analysis and the products were detected by Varian 450 GC equipped with CP-Sil 5CB (50 m, 0.32 mm, 5 μm) column and an FID detector. The calculated carbon balance was always in the range of 95–105%.

2.4 Reusability test

To investigate the stability of the catalyst, reusability tests were conducted as follows. Instead of using 0.05 g of catalyst in 5% LA/H_2O, 10 g, an excess of catalyst (0.3 g) was pretreated by using an excess of LA (30% LA/H_2O, 10 g) under standard conditions. After the pretreatment, the catalyst was filtered and washed with water and dried at room temperature for 20 h. For the first reuse experiment, 0.05 g of the pretreated catalyst was used in 5% LA/H_2O and the reaction was carried out under our standard conditions. The remaining catalyst from the first pretreatment (0.2 g) was again pretreated in 20% LA/H_2O, 10 g under standard conditions. Then the mixture was filtered, washed and dried at room temperature for 20 h. The pretreated catalyst so obtained was then used for a second reuse reaction, which was conducted in the same manner under our standard reaction conditions. For the last reusability test, once again the remaining catalyst from the second pretreatment (0.1 g) was pretreated in 10% LA/H_2O, 10 g under standard

conditions, followed with filtration, washing and drying at room temperature for 20 h. Once again, the twice pretreated catalyst obtained was used for the third reuse reaction which was conducted in the same manner as described for the earlier re-use tests.

2.5 DFT calculations

Spin unrestricted periodic DFT calculations were performed within a generalized gradient approximation using the exchange-correlation functional of Perdew, Burke and Ernzerhof (PBE)[38, 39] using the VASP program.[40-43] The core states of all atoms were represented using projector augmented wave method (PAW)[44, 45] This left 11 valence electrons per Cu atom and the usual valence levels for main group elements to be explicitly represented in the calculations. In addition dispersion interactions were included in all calculations using the Grimme D3 approach.[46]

Calculations for the interaction of molecules with Cu nanoparticles used a Cu_{75} cluster. The geometry of this Cu_{75} cluster was taken from the global optimisation studies of Dove and Wales who used Sutton Chen potentials to idientify low energy structures for a range of metallic clusters.[47] The 75 atom cluster was chosen as it provides generic features of nanoparticles including regions of (111) and (100) face centred cubic type facets as well as a low co-ordination (5-co-ordinate) Cu.

Clusters where placed in a cubic simulation cell, 25 Å on each side and a 600 eV cut-off was used to define the plane wave basis set. For cluster calculations only the Γ-point in reciprocal space was required.

A conjuguate gradient optimization procedure was used with a gradient threshold for optimization of 1.5×10^{-3} eV $Å^{-1}$. All atoms of adsorbates and cluster were optimized during the calculations and adsorption energies, E_{ads}, were calculated using the formula:

$$E_{ads} = E_{clus+X} - E_{clus} - E_X \quad (1)$$

where E_{clus+X}, is the energy of the relaxed structure of adsorbate, X, on the cluster at a given location, E_{clus}, is the optimized energy of the cluster alone and E_X, is the optimized energy of the adsorbate alone. All three calculations are carried out in the simulation repeat units with the same dimensions using the same parameters (functions, cut-off *etc*) for the calculations. We note that equation (1) will give negative energies for favorable adsorbate-cluster interactions.

3. Results and discussion

3.1 Effects of metal dopants on Cu-ZrO_2

Several catalysts were prepared by addition of metal dopants (1 wt.% each) into Cu-ZrO_2 following the impregnation procedure provided in experimental section and then tested for LA hydrogenation. For all of the catalysts the selectivity to GVL was 100% and no additional by-products were observed. Figure 1 shows that the GVL yield observed with the undoped Cu-ZrO_2 catalyst was 51% after 30 min. reaction time. To compare the performance of doped catalysts with this material GVL yield after 30 minutes of reaction was taken as a measure of catalytic activity. The addition of a secondary metal can significantly affect the catalytic performance of Cu-ZrO_2 catalysts for the hydrogenation of LA to GVL. The addition of Sc, Cr, Fe, Co, and Zn to the Cu-ZrO_2 catalyst appeared to have a detrimental effect on the catalytic performance because the observed GVL yields

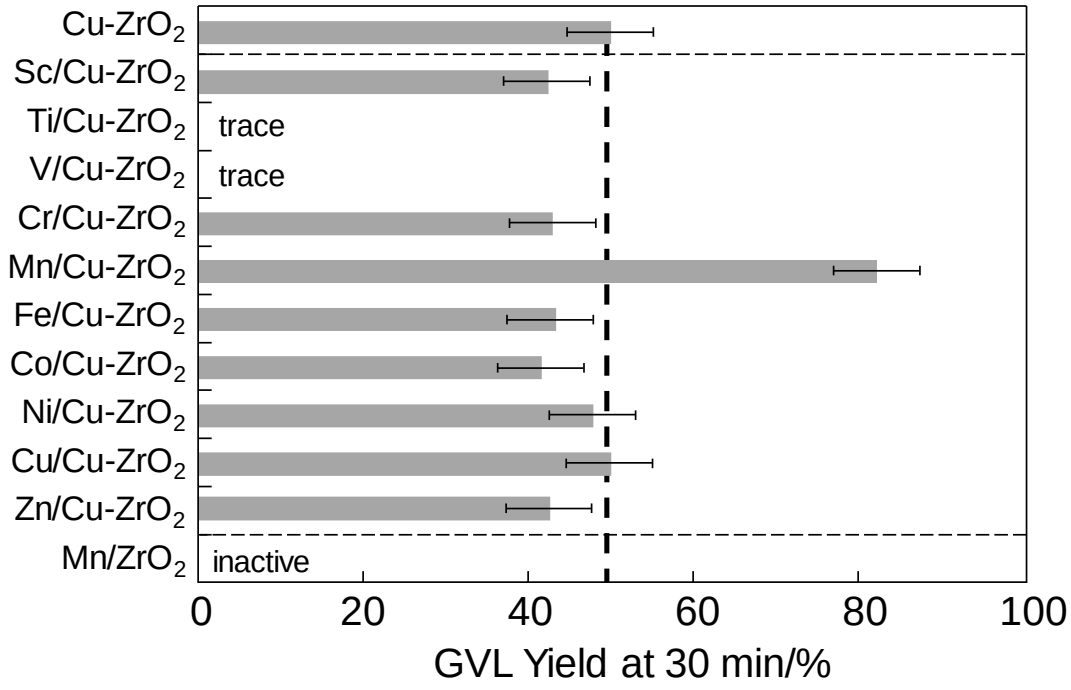

Figure 1. The effects of addition of metal dopants into Cu-ZrO_2 catalyst for the hydrogenation of LA. *Reaction conditions:* 200 °C, 0.5 h, Total pressure = 35 bar, partial pressure of H_2, p(H_2) = 26.4 bar, stirring rate 2000 rpm, substrate 5% LA/H_2O, catalyst (0.05 g). Error bars are based on the standard deviation of at least 3 repeat experiments for each data point.

for these catalysts were less than the Cu-ZrO_2 standard catalyst. At the dopant level Ni appears to have no real effect on the activity of the Cu-ZrO_2 catalyst. In previous work we have shown how incorporating significantly higher amounts of Ni at the co-precipitation preparation stage can lead to enhanced performance. The most active materials in this case consist of 45% Ni and 5% Cu co-precipitated with ZrO_2 using the oxalate gel approach.[35] Interestingly, the doping of Mn onto the Cu-ZrO_2 was found to significantly increase the yield of GVL produced (GVL yield 82%). The doping of Ti and V onto the catalyst was found to completely deactivate the Cu-ZrO_2 catalyst. It is possible that this is a result of the metal precursors used; in the case of Ti and V, metal chloride precursors were employed as the nitrate salts were not available for these two metals. The

loss of catalytic activity could imply that chlorine has poisoned the Ti/Cu-ZrO_2 and V/Cu-ZrO_2 catalysts. In order to investigate the influence of chloride on the catalytic activity, an additional Mn/Cu-ZrO_2 catalyst was prepared using $MnCl_2$ as the metal precursor and tested for the hydrogenation of LA. As with the Ti and V doped materials, the Mn/Cu-ZrO_2 was found to be inactive, highlighting the importance of the metal precursor used in the doping procedure and confirming that chlorides should be avoided.

In order to investigate the role of the Mn dopant in the Mn/Cu-ZrO_2 catalyst further, a Mn/ZrO_2 catalyst was prepared and tested under identical conditions. No activity was observed with this material, indicating Mn is acting as a dopant to enhance the activity of the Cu-ZrO_2 material rather than as a catalyst in its own right.

Table 1 summarizes the physical properties of the metals doped on Cu-ZrO_2

Table 1. Physical properties of Cu-ZrO_2 and M/Cu-ZrO_2 catalysts.

Catalyst[a]	Cu particle size[b] /nm	Cu surface area[d] /m^2 g^{-1}	BET surface area[c] /m^2 g^{-1}
Cu-ZrO_2	15	2.0	58
Sc/Cu-ZrO_2	15	1.8	42
Ti/Cu-ZrO_2	39	0.3	45
V/Cu-ZrO_2	41	0.2	51
Cr/Cu-ZrO_2	12	1.7	46
Mn/Cu-ZrO_2	12	5.4	64
Fe/Cu-ZrO_2	9	1.4	45
Co/Cu-ZrO_2	12	2.1	47
Ni/Cu-ZrO_2	8	1.6	53
Cu/Cu-ZrO_2	14	1.7	52
Zn/Cu-ZrO_2	13	2.0	44
Mn/ZrO_2	–	–	40

Notes: *a*) loading amount of metal fixed at 1 wt%., *b*) Obtained by PXRD of reduced catalyst estimated from Scherrer equation applied to the Cu metal diffraction peak at $2\theta = 43.4°$. *c*) Obtained by N_2O titration. *d*) Obtained by N_2 adsorption.

catalyst. The particle size of Cu was estimated by applying the Scherrer equation to the metallic Cu diffraction peak at 43.4° (Supplementary Information - Figure S1). With the Sc, Cr, Mn, Co, Cu, and Zn doped Cu-ZrO_2 catalysts, the particle size of Cu was determined to be approximately the same as the undoped Cu-ZrO_2 (*ca.* 15 nm). The Cu particle size associated with the Ni/Cu-ZrO_2 and Fe/Cu-ZrO_2 catalysts was found to be lower (approximately 8-9 nm). Interestingly, the catalysts prepared using the chloride precursors (V and Ti) were found to have significantly larger Cu particle sizes (*ca.* 39-41 nm), which could indicate that the excess chloride in the preparation has caused agglomeration of Cu during the calcination step used in catalyst preparation. The copper

surface area of the doped materials was estimated using an N_2O titration method. The Cu surface area associated with the standard Cu-ZrO_2 catalyst was found to be 2.0 m^2 g^{-1}. Most of the doped materials had comparable Cu surface areas in the range 1.4 m^2 g^{-1} (Fe/Cu-ZrO_2) to 5.4 m^2 g^{-1} (Mn/Cu-ZrO_2). It is notable that Mn/Cu-ZrO_2 is at the top end of this range with a measured Cu surface area more than twice that of the undoped Cu-ZrO_2 material. The catalysts formed by doping with the chloride of the metal (Ti/Cu-ZrO_2 and V/Cu-ZrO_2) have an order of magnitude lower Cu surface area, consistent with the much larger particle sizes observed from XRD analysis. In order to ensure that the copper surface area measurement for the Mn/Cu-ZrO_2 was as accurate as possible, another measurement was conducted with Mn doped onto zirconia without any co-precipitated Cu, Mn/ZrO_2. No adsorption of N_2O was observed for Mn/ZrO_2 and so we conclude that all of the N_2O adsorbed by the Mn/Cu-ZrO_2 material was due to the interaction with surface Cu species. The measured BET surface areas for all materials were found to fall in a narrow range (40-64 m^2 g^{-1}), suggesting that the doping of Cu-ZrO_2 with a second metal has little effect on the microstructure of the synthesized catalysts.

3.2 The effect of the Mn dopant loading on catalyst structure and activity.

As discussed in Section 3.1, the only dopant that resulted in a significant increase in the GVL yield under our standard testing conditions was Mn. Accordingly, further tests were carried out to attempt to optimize the Mn loading. A series of materials was prepared with various amounts of Mn dopant in the Cu-ZrO_2 catalyst and these were tested for the hydrogenation of LA to GVL using our standard conditions. The measured GVL yield as a function of Mn dopant level between 0 and 1.5 % is shown in Figure 2a. It is clear that the dopant level of Mn has a significant effect on the catalytic activity. The highest activity for the Mn/Cu-ZrO_2 system was with a 1 wt.% Mn loading. Figure 2b shows how the Cu crystallite size and Cu surface area are affected by the incorporation of differing quantities of Mn dopant. The Cu particle size did not change up to a Mn loading of 0.5 wt.%.

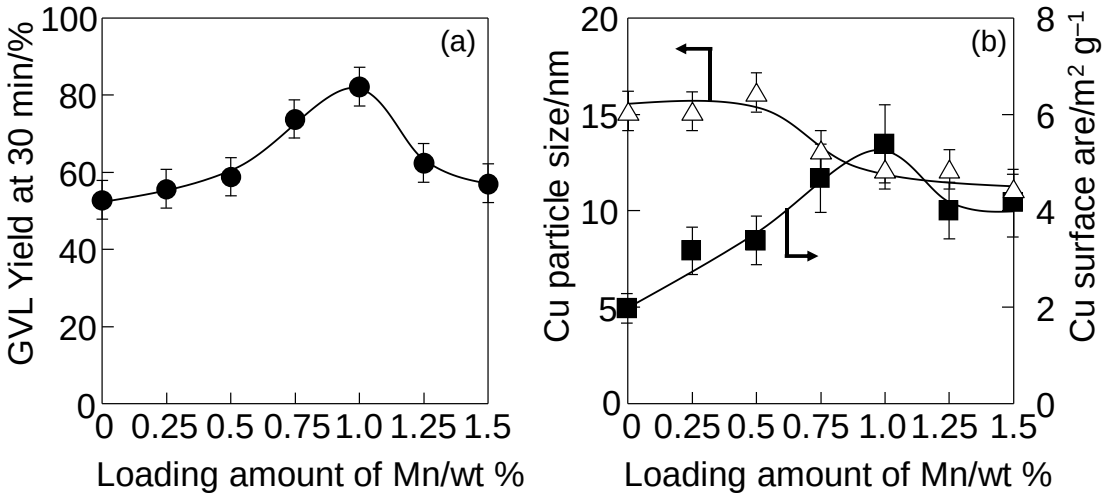

Figure 2. Dependences of (a) GVL yield and (b) particle size of Cu and Cu surface area on Mn loading on Mn/Cu-ZrO_2. *Reaction conditions:* 200 °C, Total pressure = 35 bar, partial pressure of H_2, p(H_2) = 26.4 bar, stirring rate 2000 rpm, substrate 5% LA/H_2O, catalyst (0.05 g). Cu particle size obtained by PXRD of reduced catalyst estimated from Scherrer equation applied to the Cu metal diffraction peak at 2θ = 43.4°. Cu surface area obtained by N_2O titration. Error bars are based on the standard deviation of at least 3 repeat experiments for each data point.

However, as the wt.% of Mn in the system exceeded 0.75 wt.%, the Cu crystallite size decreased to approximately 12 nm before a plateau was reached with Mn >1 wt.%. Interestingly, the copper surface area followed a very similar trend to the catalytic performance and reached a maximum at 1 wt. % Mn. This suggests that the catalytic performance was affected by Cu surface area and that the role of Mn may be to assist with the dispersion of Cu on the surface of the catalyst. Indeed, we have already noted that the highest Cu surface area in our survey of first row transition metal dopants occurs for Mn/Cu-ZrO_2 (Table 1). Mn loadings exceeding 1 wt.% have a detrimental effect on both the catalytic performance and the measured Cu surface area.

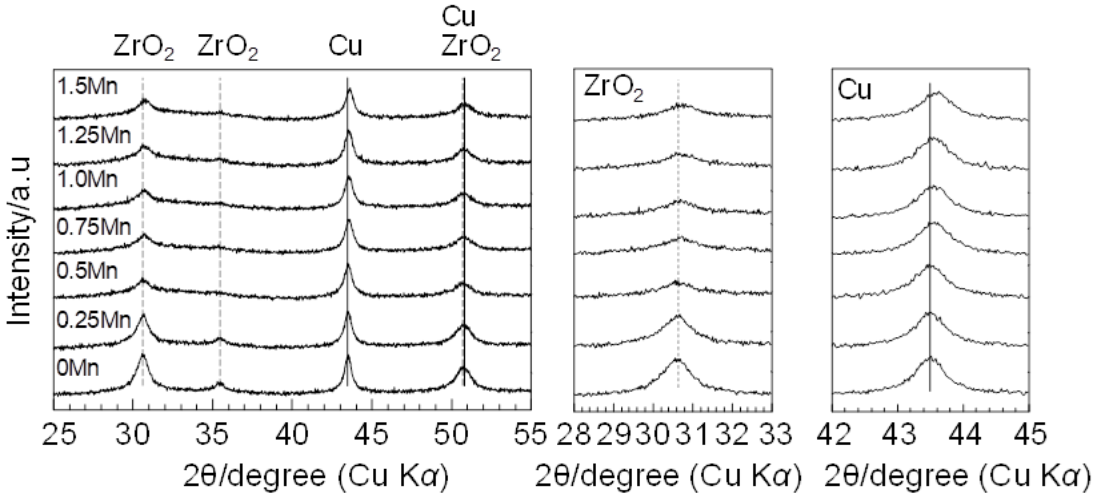

Figure 3. PXRD patterns of 0-1.5 wt% Mn on Cu-ZrO_2 catalysts; Dash line and solid line corresponding to ZrO_2 and Cu, respectively.

The effect of Mn doping on the phases contained in the Mn/Cu-ZeO_2 catalysts was investigated using PXRD. Figure 3 shows the changes in the PXRD patterns for the Mn/Cu-ZrO_2 samples after impregnation with various amounts of Mn dopant. The intensity of the main PXRD peak corresponding to the ZrO_2 phase (30.6º) in the Mn/Cu-ZrO_2 catalyst gradually decreased with an increase in the amount of Mn up to a loading

of 0.5 wt%. However, this effect was not observed on further increase in the amount of Mn added to the Cu-ZrO_2 material. This data indicates that the ZrO_2 phase in the Cu-ZrO_2 catalyst becomes increasingly amorphous with addition of increasing amounts of the Mn dopant up to a loading of 0.5 wt%. On the other hand, there was no change or shift of the diffraction peaks related to metallic Cu (around 43.5°) up to 0.5 wt% of Mn. Further increases in the loading of Mn above 0.5 wt% resulted in a slight decrease in intensity of this reflection for metallic Cu and also a small shift of the peak to higher diffraction angles, which may indicate that Mn has been incorporated into the metallic Cu particles. So, at these higher levels of the Mn dopant, a significant influence on the structure of the metallic Cu nanoparticles can be observed. From these results, we conclude that the introduction of the Mn dopant results in a lowering of crystallinity of the ZrO_2 phase in the Cu-ZrO_2 and above 0.5 wt% the structural effect of the Mn dopant on the Cu metallic phase becomes detectable by PXRD.

Figure S2 (Supplementary Information) shows an SEM image and the elemental distribution from the corresponding EDX spectra for a representative 600 nm scale agglomeration of particles for the 1 wt% Mn/Cu-ZrO_2 catalyst. At the scale shown, the three metals present (Zr, Cu and Mn) are uniformly distributed over the sample.

3.3 The effect of the 1 wt %Mn dopant on the catalytic performance of Mn/Cu-ZrO_2.

Figure 4 compares GVL yield as a function of time for the 1 wt% Mn/Cu-ZrO_2 sample and the standard Cu-ZrO_2 catalyst. It is clear that the Mn/Cu-ZrO_2 catalyst has a significantly higher initial rate than the standard Cu-ZrO_2 catalyst. Full conversion of LA into GVL was obtained after only 45 minutes with the optimized Mn/Cu-ZrO_2 catalyst whereas this is only reached at 90 minutes for the same mass of the Cu-ZrO_2 material. The effect of Mn doping on the rate of reaction was estimated from the formation rate of GVL in the initial stage of the reaction from 0 to 15 mins (inset into Figure 4), the rate of reaction catalyzed by Mn/Cu-ZrO_2 was found to be 1.6 times higher than that with the

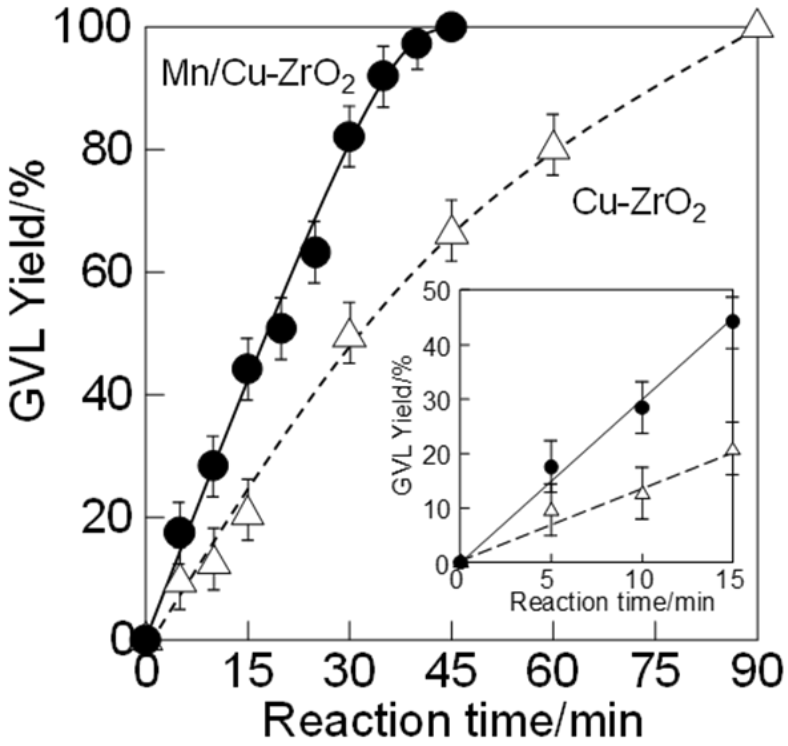

Figure 4. Time online data for the hydrogenation of LA to GVL over (△) Cu-ZrO_2 and (●) 1 wt.% Mn/Cu-ZrO_2. *Reaction conditions*: 200 °C, Total pressure = 35 bar, partial pressure of H_2, p(H_2) = 26.4 bar, stirring rate 2000 rpm, substrate 5% LA/H_2O, catalyst (0.05 g). Error bars are based on the standard deviation of at least 3 repeat experiments for each data point.

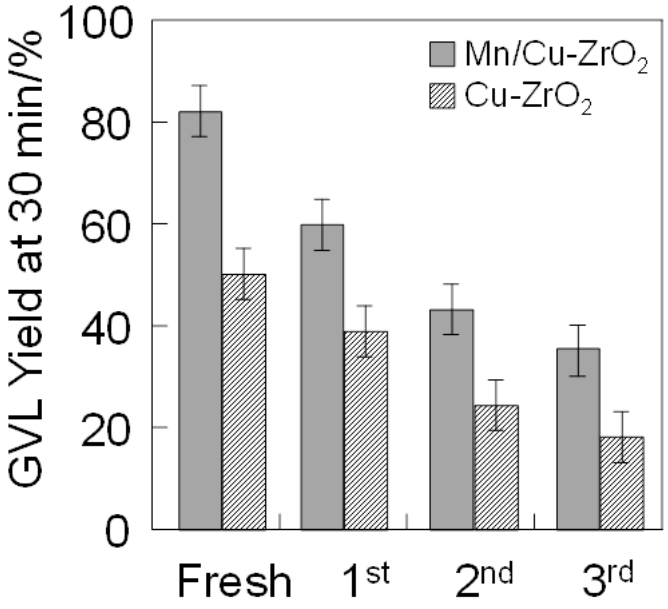

Figure 5. Reusability assessment of Cu-ZrO_2 and Mn/Cu-ZrO_2 for the hydrogenation of LA to GVL. *Reaction conditions*: 200 °C, Total pressure = 35 bar, partial pressure of H_2, p(H_2) = 26.4 bar, stirring rate 2000 rpm, substrate 5% LA/H_2O, catalyst (0.05 g). Error bars are based on the standard deviation of at least 3 repeat experiments for each data point.

standard Cu-ZrO_2 catalyst. Figure 4 also shows that the GVL yield increases linearly with time for both Cu-ZrO_2 and Mn/Cu-ZrO_2 catalysts up to 30 minutes and so confirms that the GVL yield at this time can be taken as an indicator of the catalyst activity.

In order to assess the stability of the catalyst, a reusability test was conducted following the procedure detailed in the experimental section. Figure 5 reveals how the Mn/Cu-ZrO_2 and the undoped Cu-ZrO_2 catalysts performed over successive reuse experiments in terms of the measured activity from GVL yield at 30 min reaction time. A significant loss in activity was observed on reuse for both types of catalyst. The undoped Cu-ZrO_2, activity reduced from 50 % to only 18 % GVL yield at 30 min reaction time between the first and third use of the catalyst sample. Similarly, the Mn/Cu-ZrO_2 catalyst showed a reduction in activity from 82 % to 36 % GVL yield at 30 min reaction time.

Figure S3 (in Supplementary Information) shows the PXRD patterns of the undoped Cu-ZrO_2 and Mn/Cu-ZrO_2 catalysts both before use and after the third reuse reaction (dried at room temperature between reuse runs). The intensity of the reflection associated with metallic Cu (43.4°) appears to decrease following use of the catalyst. In our earlier paper using co-precipitated Cu-ZrO_2 catalysts leaching studies showed very low loss of Cu under our reaction conditions[35] and so metal leaching is not responsible for the observed loss of activity on re-use. Leaching tests were also carried out for the Mn/Cu-ZrO_2 catalysts and similarly low levels of Cu leaching where observed (100 ppm). To check the effect of this level of homogeneous metal we also ran an additional test: After 20 minutes of reaction (GVL yield 50 %) the autoclave was cooled and depressurised and then the catalyst was filtered off. The filtrate was then returned to the autoclave and the reaction continued under normal reaction conditions (except for the absence of the solid catalyst). No further conversion was observed after an additional 30 minutes, confirming that the active catalyst is heterogeneous.

Figure S3 also shows additional reflections in the diffraction pattern are seen after third reuse compared to the pattern of the fresh material. These additional peaks indicate that Cu_2O is present in the used material. This implies that the decline in catalytic performance was a result of Cu oxidation into Cu_2O following the reaction which is consistent with the idea that reduction of copper oxide species into copper metal (during reaction) is an important step in the catalytic process.[31] Ex-situ treatment of the re-used material with H_2 did lead to the reduction of this Cu_2O as evidenced by the loss of the Cu oxide features and enhancement of Cu metal. Even so catalytic activity was not restored. This suggests that agglomeration of Cu during the reaction process may make these Cu_2O particles both more difficult to re-activate on re-use and to loose activity due to sintering.

3.4 Comparison of reaction kinetic parameters for LA hydrogenation over Mn/Cu-ZrO_2 and Cu-ZrO_2 catalysts

As discussed in the previous section, doping of Mn into Cu-ZrO_2 significantly improved the GVL yield observed after 30 min reaction time. Characterisation of the synthesized materials shows that Mn doping causes an increase in the Cu surface area. In order to probe the effect of Mn doping further, a kinetic study was carried out to determine the order of reaction with respect to each of the reactants (H_2 and LA). We also estimated the apparent activation energies for each of the catalysts (Cu-ZrO_2 and Mn/Cu-ZrO_2) from the initial rates of reactions carried out at different temperatures. Figure 6 shows the measured rate constant as a function of LA concentration and as a function of H_2 partial pressure over Cu-ZrO_2 and Mn/Cu-ZrO_2 catalysts. For both catalysts, the reaction order observed with respect to LA concentration was approximately zero (figure 6*a*). In the case of H_2 partial pressure for the Cu-ZrO_2 catalyst the results were first plotted as a function of total pressure on a linear scale (Figure S4) and a linear fit used to confirm the autogeneous pressure of 8.6 bar that was observed during the heating stage of the experiment prior to pressurizing with H_2. This allowed us to extract an accurate partial pressure of H_2 for calculating the order of reaction. With respect to the partial pressure of H_2 (P_{H2}), different reaction orders were observed for the Mn/Cu-ZrO_2 and Cu-ZrO_2 catalysts. Figure 6*b* shows that the Cu-ZrO_2 catalyst gives an estimated order of 1.0 with respect to p(H_2), suggesting that the H_2 adsorption and dissociation on the Cu surface is a limiting step in the hydrogenation process. Whereas, the reaction order with respect to P_{H2} using the Mn/Cu-ZrO_2 catalyst is 0.3, suggesting that the performance of this catalyst is not limited by the pressure of H_2 to the same extent.[14] In addition, extrapolation of the linear fit of reaction rate with respect to total pressure did not give agreement with the

autogeneous pressure measured at the start of the reaction (Figure S4), again suggesting that the dependence on H_2 partial pressure is of low order. This result suggests that H_2 adsorption (dissociative adsorption) is rapid compared to other steps in the hydrogenation reaction as may be expected given the high Cu surface area measured using N_2O adsorption (Table 1). For Ru/C catalysts a near zero reaction order with respect to LA has also been reported along with a dependence on $p(H_2)$ of 0.5.[14]

TPR profiles for freshly calcined Cu-ZrO_2, Mn/Cu-ZrO_2 and Mn/ZrO_2 materials are

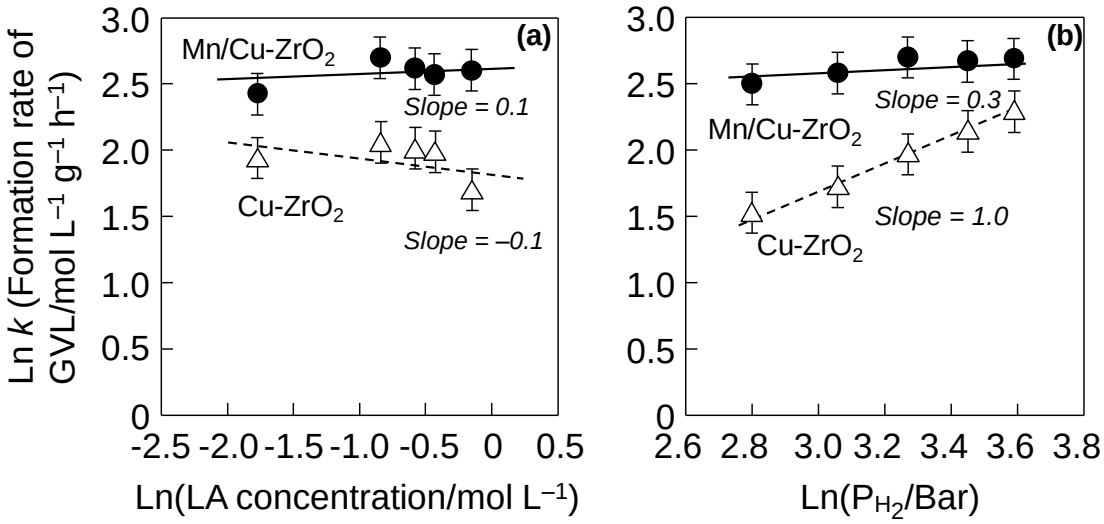

Figure 6. Effect of (a) concentration of LA with total pressure = 35 bar, partial pressure of H_2, $p(H_2)$ = 26.4 bar, and (b) hydrogen partial pressure, $p(H_2)$ with substrate 5% LA/H_2O, on the hydrogenation of LA over (△) Cu-ZrO_2 and (●) Mn/Cu-ZrO_2. *Reaction conditions:* 200 °C, 0.25 h, stirring rate 2000 rpm, catalyst (0.05 g). Error bars are based on the standard deviation of at least 3 repeat experiments for each data point.

presented in Figure S5 (Supplementary Information). For Mn/ZrO_2 (without Cu), no TPR peak was detected in the temperature program range (50-400 °C). Although there are literature reports of TPR peaks corresponding to Mn species below 400 °C,[37-40] the amount of Mn present in our samples is likely to lead to hydrogen adsorption in the TPR experiment below the detection limit of the instrument. For the Cu containing catalysts,

the temperature at which we observe the TPR peak and the area beneath the reduction feature is practically the same for both of the catalysts (Cu-ZrO_2 and Mn/Cu-ZrO_2). These results, suggest that Mn doping does not significantly affect the reduction of oxidized copper contained in these materials.

We have also carried out the hydrogenation reaction at a series of temperatures to produce an Arrhenius plot of the reaction rate constant in the presence of each of the catalysts (Cu-ZrO_2 and Mn/Cu-ZrO_2) and the data is presented in Figure 7. The activation energies calculated from these plots are 69.0 kJ mol^{-1} (Cu-ZrO_2) and 45.7 kJ mol^{-1} (Mn/Cu-ZrO_2), so that the addition of Mn dopant appears to lower the activation energy for hydrogenation of LA to GVL using Cu-ZrO_2 catalysts. This estimated activation

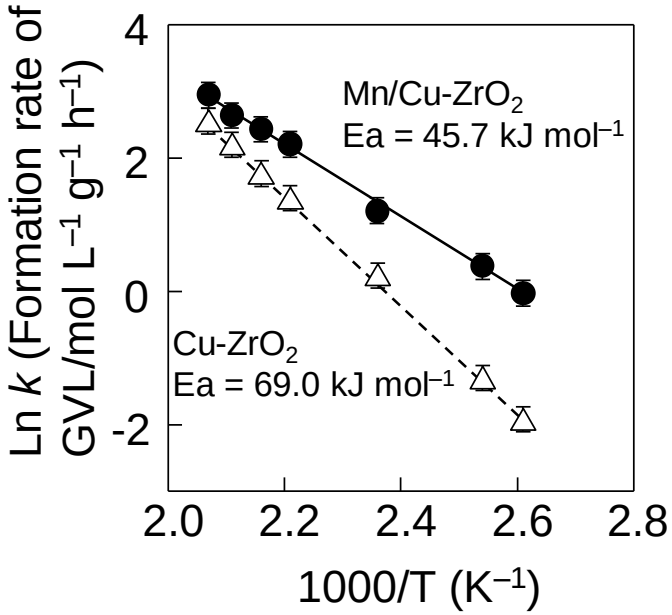

Figure 7. Arrhenius plot of the hydrogenation of LA over (△) Cu-ZrO_2 and (●) Mn/Cu-ZrO_2. *Reaction conditions*: 110 - 200 °C, total pressure = 35 bar, partial pressure of H_2, p(H_2) = 26.4 bar, 0.5 h, stirring rate 2000 rpm, substrate 5% LA/H_2O, catalyst (0.02 - 0.05 g). Error bars are based on the standard deviation of at least 3 repeat experiments for each data point.

energy with the Mn/Cu-ZrO_2 catalyst is similar to the activation energy for the hydrogenation of LA to GVL using a Ru/C catalyst (48 kJ mol^{-1}) reported previously.[14]

3.5 Isotope labelling experiments and DFT calculations relevant to hydrogenation mechanism

Isotope labelling studies were undertaken for the LA to GVL reaction using our most active catalyst, 1wt% Mn/Cu-ZrO_2. The results were analysed using ^{13}C and ^{1}H NMR. ^{13}C NMR for the product of hydrogenation in H_2O and D_2O solvents are compared in Figure S6. In agreement with earlier work on Ru/C[20] we note that the relative ^{13}C NMR signals for the ^{13}C atom at the 4 position and that for ^{13}C at the 2 position in the GVL product is significantly lower when D_2O solvent is used compared to H_2O. Following Scheme 1 the C atom at the 4 position will be hydrogenated as the HPA (**2**) intermediate is formed and so this result indicates that D originating from the D_2O solvent is involved in the hydrogenation step of the reaction. Checks subjecting GVL to the same reaction conditions showed no evidence of deuterium exchange between the product and solvent. In contrast to the labelling results reported for Ru/C we also see reduction in the signals for ^{13}C at positions 3 and 5 relative to ^{13}C at position 2 when Mn/Cu-ZrO_2 catalysts are used.

To attempt to quantify the extent of H/D exchange during the hydrogenation reaction we turned to ^{1}H NMR. The resulting spectra are presented in Figures S7 and the peak integration information is given in Tables S1. Unfortunately the ^{1}H NMR signal for the proton at C4 is obscured by a broad solvent peak. However, the results confirm that there is H/D exchange of hydrogen at C3 and C5 in the GVL product and also show that C3 and C5 in the residual LA substrate have undergone H/D exchange. This was also found in an experiment carried out under the same conditions but with no catalyst present for

which no conversion of LA was observed but H/D exchange at C3 and C5 was still evident (Figure S8 and Table S2). Similar experiments carried out at the lower temperatures used with Ru catalysts show no such H/D exchange at C3 and C5.

Exchange of H and D at C3 and C5 suggests that the LA substrate will undergo enolisation under the reaction conditions used with Cu-ZrO_2 catalysts and so the reaction scheme should be modified as shown in Scheme 2 to include enolisation to either the C3-enol, **4**, or C4-enol, **5**. There is then the additional possibility of hydrogenation at the C=C bond of enol isomers **4**/**5** to produce the HPA intermediate.

The ^{13}C results also suggest that the H species used in the hydrogenation of LA to GVL could be derived from the H_2O/D_2O solvent. We note that H-spillover and reverse spillover phenomena, in which there is H/D exchange between atomic H on Cu nanoparticles and hydroxyl groups on an oxide support have been investigated for methanol synthesis from CO/CO_2 using Cu/ZrO_2 catalysts.[48] Recent DFT calculations have also shown that this type of process is both thermodynamically and kinetically quite facile for Cu_4 nanoparticles supported on hydroxylated SiO_2.[49] H-spillover and rapid

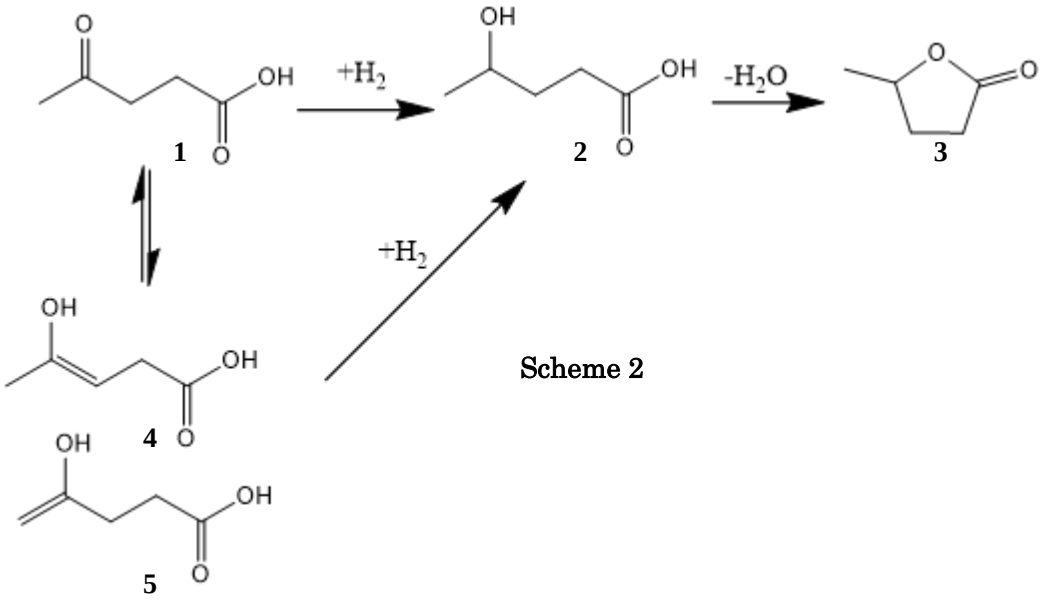

Scheme 2

exchange between the water solvent and surface hydroxyls would provide a route for the atomic H formed on the Cu nanoparticles of the Mn/Cu-ZrO_2 to be scrambled with D from the D_2O solvent.

3.6 DFT calculations regarding ketone/enol adsorption at Cu_{75} nanoparticles.

The calculated adsorption energies for the species shown in Scheme 2 on the Cu_{75} model nanoparticle are given in Table 2. The structure of the nanoparticle and the adsorbed molecules are shown in Figure S9. Three locations on the nanoparticle were used in these calculations Cu_{75}(111) and Cu_{75}(100) facets and the apical atom which is five co-ordinate, Cu_{75}(5-fold). We observe that for all species considered the adsorption energy is most negative (favourable) on the Cu_{75}(5-fold) site than on the facets with the Cu_{75}(111) facet giving the lowest energy adsorption in all cases. For LA, **1**, adsorption by the acid and ketone functionalities was compared and only the most favourable cases are reported here. Figure S9 shows that adsorption of LA via the ketone group is preferred on the facets but for the Cu_{75}(5-fold) site LA adsorbs preferentially via the acid group. For both the C3-enol, **4** and the C4-enol, **5** adsorption via the C=C π-bond is always preferred over the other functional groups of these molecules. In fact the enol adsorption is significantly stronger than seen for LA (up to 38.8 kJ mol^{-1} more negative for the Cu_{75}(5-fold) site). This suggests that the enolisation that has been observed under the reaction conditions used of the Cu-ZrO_2 based catalysts will increase the surface concentration of the substrate on the Cu nanoparticle surfaces. We also note that the adsorption energy of the enol isomers is considerably more favourable than that of the GVL product. This would suggest that enolisation will also reduce any product inhibition effects.

Table 2. Calculated adsorption energies for species shown in Scheme 2 at sites on a Cu_{75} nanoparticle.

Adsorbed species	**Adsorption sites**		
	$Cu_{75}(111)$ / kJ mol^{-1}	$Cu_{75}(100)$ / kJ mol^{-1}	Cu_{75}, 5- fold / kJ mol^{-1}
LA, **1**	-45.0	-64.5	-74.6
C4-enol, **5**	-86.5	-98.9	-113.4
C3-enol, **4**	-65.3	-90.1	-103.6
HPA, **2**	-54.2	-74.6	-73.1
GVL, **3**	-52.4	-66.4	-85.6

3.7 The effect of water concentration on reaction rate.

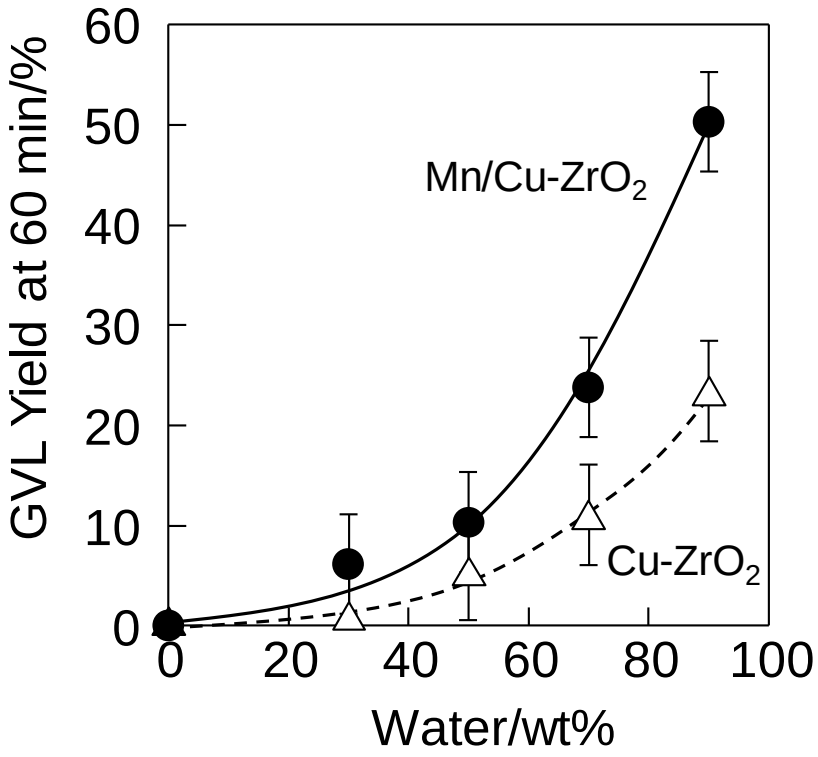

Figure 8. Dependence of GVL yield on amount of water solvent used for (△) Cu-ZrO_2 and (●) Mn/Cu-ZrO_2. *Reaction conditions*: 200 °C, total pressure = 35 bar, partial pressure of H_2, p(H_2) = 26.4 bar, stirring rate 2000 rpm, 1 h, substrate 30-100% LA/H_2O, catalyst (0.05 g). Error bars are based on the standard deviation of at least 3 repeat experiments for each data point.

The observation that water is implicated in the hydrogenation step of this reaction, providing at least some of the H-species used, led us to investigate the effect of water on the catalytic activity of both doped and undoped catalysts. Figure 8 shows the effect of water on GVL yield after 60 minutes of reaction. The amount of LA in the reaction was fixed at 1 g (8.6 mmol), and the dose of water in the reactor was changed from zero to 9 ml (0-90 wt. %). The GVL yield increased with an increase in the amount of water in the reaction solution. The data clearly indicate that water contributes to the hydrogenation of LA over both doped and undoped catalysts. The contribution of water in the reaction was calculated from the slope of the activity and the contribution of water over the Mn/Cu-ZrO_2 was found to be larger than that of undoped Cu-ZrO_2 catalyst.

Conclusions

The development of Cu-ZrO_2 catalyst for the catalytic hydrogenation of LA to form GVL by the addition of various dopant oxides (Sc, Ti, V, Cr, Mn, Fe, Co, Ni, Cu, and Zn) was investigated. Impregnation of 1wt.% Mn in the Cu-ZrO_2 significantly increased the catalytic activity, and the catalyst was found to be 1.6 times more active than that of undoped Cu-ZrO_2 catalyst. The role of Mn dopant on the Cu-ZrO_2 catalyst was investigated in terms of physical property of Cu as the catalytically active component and found out that the quantity of Mn in the catalyst system has a significant effect on the catalytic activity. The activity of the Mn/Cu-ZrO_2 system was highest with a 1 wt.% Mn loading. Interestingly, the copper surface area followed a very similar trend to the catalytic performance and reached a maximum at 1 wt. % Mn. This suggests that the catalytic performance is proportional to the Cu surface area of the material and the role of the Mn is to assist with the dispersion of Cu on the surface of the catalyst.

Furthermore, a kinetic study was carried out identifying the order of reaction for both reactants (H_2 and LA) and the activation energies for Cu-ZrO_2 and Mn/Cu-ZrO_2 catalysts. The reaction order observed with respect to LA concentration was approximately zero both for doped and undoped catalysts. With respect to the pressure of H_2 in the system however, different reaction orders were observed for the Mn/Cu-ZrO_2 and Cu-ZrO_2 catalysts. The lower reaction order in the presence of dopant-Mn suggests that H_2 adsorption (dissociative adsorption) is rapid, such that the surface reactions involving the addition of atomic hydrogen to adsorbed LA controls the rate of LA hydrogenation. A comparable reaction order with respect to H_2 to that found for the Mn/Cu-ZrO_2 material has previously been reported with Ru catalysts. The activation energy for the hydrogenation reaction was also found to be lower for Mn/Cu-ZrO_2 than for undoped Cu-ZrO_2 (45.7 kJ mol^{-1} *cf*. 69.0 kJ mol^{-1}).

NMR analysis of reactions carried out in D_2O and H_2O using a combination of ^{13}C-NMR and ^{1}H-NMR show that water is important in the catalytic mechanism of the reaction. Under the reaction conditions used here these experiments also demonstrated that enolisation of the LA takes place, whereas no enolisation is observed under the milder conditions commonly used with Ru catalysts. DFT calculations suggest that this observation is important as the enol isomers of LA are found to adsorb more strongly to the surface sites of a model Cu_{75} nanoparticle.

Overall we have demonstrated that there is further scope to optimize the Cu-ZrO_2 catalysts for the LA to GVL hydrogenation reaction. This may lead to materials that are competitive with the established Ru materials but with the advantages of sustainability.

Supplementary Information

Contents: Powder XRD patterns of materials, SEM images, detailed plots for reaction order assessment, TPR and NMR analysis along with DFT calculated structures.

Acknowledgement

This work was financially supported by the European Union FP7 NMP project NOVACAM (Novel cheap and abundant materials for catalytic biomass conversion, FP7-NMP-2013- EU-Japan-604319). Via our membership of the UK's HEC Materials Chemistry Consortium, which is funded by EPSRC (EP/L000202), this work used the ARCHER UK National Supercomputing Service (http://www.archer.ac.uk). Computing resource was also provided by Advanced Research Computing at Cardiff (ARCCA) and the HPC-Wales supercomputer facilities.

References

1. Corma, A.; Iborra, S.; Velty, A. Title. *Chem. Rev.* **2007**, *107*, 2411-2502.
2. Ruppert, A. M.; Weinberg, K.; Palkovits, R. Title. *Angew. Chem., Int. Ed.* **2012**, *51*, 2564-2601.
3. Serrano-Ruiz, J. C.; Dumesic, J. A. Title. *Energy Environ. Sci.* **2011**, *4*, 83-99.
4. Fang Q.; Hanna M. A. Title. *Bioresour Technol*. **2002**, *81*, 187-192.
5. Horvath I. T.; Mehdi H.; Fabos V.; Boda L.; Mika L. T. Title. *Green Chem.* **2008**, *10*, 238-242.
6. Ismalaj E.; Strappaveccia G.; Ballerini E.; Elisei F.; Piermatti O.; Gelman D.; Vaccaro L. Title. *ACS Sustainable Chem. Eng.* **2014**, *2*, 2461-2464.
7. Liguori F.; Moreno-Marrodan C.; Barbaro P. Title. *ACS Catal.* **2015**, *5*, 1882-1894.
8. Chalid M.; Broekhuis A. A.; Heeres H. J. Title. *J. Mol. Catal. A: Chem.* **2011**, *341*, 14-21.
9. Deng L.; Li J.; Lai D.-M.; Fu Y.; Guo Q.-X **Title**. *Angew. Chem., Int. Ed.* **2009**, *48*, 6529-6532, S6529/6521-S6529/6524.
10. Fabos V.; Mika L. T.; Horvath I. T. Title. *Organometallics* **2014**, *33*, 181-187.
11. Geilen F. M. A.; Engendahl B.; Harwardt A.; Marquardt W.; Klankermayer J.; Leitner W. Title. *Angew. Chem., Int. Ed.*, **2010**, *49*, 5510-5514, S5510/5511-S5510/5510.
12. Li W.; Xie J.-H.; Lin H.; Zhou Q.-L. *Green Chem.* Title. **2012**, *14*, 2388-2390.
13. Tukacs J. M.; Novak M.; Dibo G.; Mika L. T. Title. *Catal. Sci. Technol.* **2014**, *4*, 2908-2912.
14. Abdelrahman O. A.; Heyden A.; Bond J. Q. Title. *ACS Catal.* **2014**, *4*, 1171-1181.

15. Al-Shaal M. G.; Wright W. R. H.; Palkovits R. Title. *Green Chem.*, **2012**, *14*, 1260-1263.
16. Hengne A. M.; Kamble S. B.; Rode C. V. Title. *Green Chem.*, **2013**, *15*, 2540-2547.
17. Luque R.; Clark J. H. Title. *Catal. Commun.*, **2010**, *11*, 928-931.
18. Manzer L. E. Title. *Appl. Catal., A*, **2004**, *272*, 249-256.
19. Sudhakar M.; Lakshmi Kantam M.; Jaya V. S.; Kishore R.; Ramanujachary K. V.; Venugopal A. Title. *Catal. Commun.*, **2014**, *50*, 101-104.
20. Tan J.; Cui J.; Deng T.; Cui X.; Ding G.; Zhu Y.; Y. Li Title. *ChemCatChem*, **2015**, *7*, 508-512.
21. Yan Z.-P.; Lin L.; Liu S. Title. *Energy Fuels*, **2009**, *23*, 3853-3858.
22. Du X.-L.; He L.; Zhao S.; Liu Y.-M.; Cao Y.; He H.-Y.; Fan K.-N. Title. *Angew. Chem., Int. Ed.*, **2011**, *50*, 7815-7819, S7815/7811-S7815/7811.
23. Son P. A.; Nishimura S.; Ebitani K. Title. *RSC Adv.*, **2014**, *4*, 10525-10530.
24. Yan K.; Lafleur T.; Wu G.; Liao J.; Ceng C.; Xie X. Title. *Appl. Catal., A*, **2013**, *468*, 52-58.
25. Kumar V. V.; Naresh G.; Sudhakar M.; Anjaneyulu C.; Bhargava S. K.; Tardio J.; Reddy V. K.; Padmasri A. H.; Venugopal A. Title. *RSC Adv.*, **2016**, *6*, 9872-9879.
26. Hengne A. M.; Kadu B. S.; Biradar N. S.; Chikate R. C.; Rode C. V. Title. *RSC Adv.*, **2016**, *6*, 59753-59761.
27. Shimizu K.-I.; Kanno S.; Kon K. Title. *Green Chem.*, **2014**, *16*, 3899-3903.
28. Li W.; Fan G.; Yang L.; Li F. Title. *ChemCatChem*, **2016**, *8*, 2724-2733.
29. Kumar V. V.; Naresh G.; Sudhakar M.; Tardio J.; Bhargava S. K.; Venugopal A. Title. *Appl. Catal., A*, **2015**, *505*, 217-223.
30. Q. Xu, X. Li, T. Pan, C. Yu, J. Deng, Q. Guo and Y. Fu Title. *Green Chem.*, 2016, 18, 1287-1294.
31. Ishikawa S.; Jones D. R.; Iqbal S.; Reece C.; Morgan D. J.; Willock D. J.; Miedziak P. J.; Bartley J. K.; Edwards J. K.; Murayama T.; Ueda W.; Hutchings G. J. Title. *Green Chem.*, **2017**, *19*, 225-236.
32. Hengne A. M.; Rode C. V. Title. *Green Chem.*, **2012**, *14*, 1064-1072.
33. Putrakumar B.; Nagaraju N.; Kumar V. P.; Chary K.V. R. Title. *Catal. Today*, **2015**, *250*, 209-217.
34. Jones D. R.; Iqbal S.; Ishikawa S.; Reece C.; Thomas L. M.; Miedziak P. J.; Morgan D. J.; Edwards J. K.; Bartley J. K.; Willock D. J.; Hutchings G. J. Title. *Catal. Sci. Technol.*, **2016**, *6*, 6022-6030.
35. Jones D. R.; Iqbal S.; Thomas L.; Ishikawa S.; Reece C.; Miedziak P. J.; Morgan D. J.; Bartley J. K.; Willock D. J.; Ueda W.; Hutchings G. J. Title. *Catal., Struct. React.*, **2018**, *4*, 12-23.
36. Zhang X.-R.; Wang L.-C.; Yao C.-Z.; Cao Y.; Dai W.-L.; He H.-Y.; Fan K.-N. Title. *Catal. Lett.*, **2005**, *102*, 183-190.
37. Yao C.-Z.; Wang L.-C.; Liu Y.-M.; Wu G.-S.; Cao Y.; Dai W.-L.; He H.-Y.; Fan K.-N. Title. *Appl. Catal., A*, **2006**, *297*, 151-158.

38. Perdew J. P.; Burke K.; Ernzerhof M. Generalized Gradient Approximation Made Simple. *Phys. Rev. Lett.*. **1996**, *77*, 3865-3868.
39. J. P. Perdew, K. Burke and M. Ernzerhof, *Phys. Rev. Lett.* Generalized Gradient Approximation Made Simple. **1997**, *78*, 1396-1396.
40. Kresse G.; Hafner J. Title. *Phys. Rev. B: Condens. Matter*, **1993**, *47*, 558-561.
41. Kresse G.; Hafner J. Title. *Phys. Rev. B: Condens. Matter*, **1994**, *49*, 14251-14269.
42. Kresse G.; Furthmuller J. Title. *Comput. Mater. Sci.*, **1996**, *6*, 15-50.
43. Kresse G.; Furthmueller J. Title. *Phys. Rev. B: Condens. Matter*, **1996**, *54*, 11169-11186.
44. Bloechl P. E., Title. *Phys. Rev. B: Condens. Matter*, **1994**, *50*, 17953-17979.
45. Kresse G.; Joubert D. Title. *Phys. Rev. B: Condens. Matter Mater. Phys.*, **1999**, *59*, 1758-1775.
46. Grimme S.; Antony J.; Ehrlich S.; Krieg H. Title. *J. Chem. Phys.*, **2010**, *132*, 154104/154101-154104/154119.
47. Doye J. P. K.; Wales D. J., Title. *New J. Chem.*, **1998**, *22*, 733-744.
48. Jung K.-D.; Bell A. T. Title. *J. Catal.*, **2000**, *193*, 207-223.
49. Maleki F.; Schlexer P.; Pacchioni G. Title. *Surf. Sci.*, **2018**, *668*, 125-133.